Physics of Fluids

Modeling of dispersion of aerosolized airborne pathogens exhaled in indoor spaces

Cite as: Phys. Fluids **35**, 047105 (2023); https://doi.org/10.1063/5.0142869
Submitted: 18 January 2023 • Accepted: 15 March 2023 • Published Online: 04 April 2023

Praveen Sharma, Supreet Singh Bahga and Amit Gupta

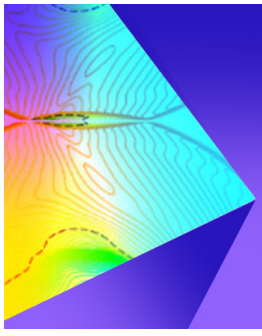

AIP Publishing

Physics of Fluids ARTICLE scitation.org/journal/phf

Modeling of dispersion of aerosolized airborne pathogens exhaled in indoor spaces

Cite as: Phys. Fluids **35**, 047105 (2023); doi: 10.1063/5.0142869
Submitted: 18 January 2023 · Accepted: 15 March 2023 ·
Published Online: 4 April 2023

Praveen Sharma,[1,2] Supreet Singh Bahga,[1] and Amit Gupta[1,a)]

AFFILIATIONS

[1]Department of Mechanical Engineering, Indian Institute of Technology Delhi, Hauz Khas, New Delhi 110016, India
[2]Military Engineer Services, Ministry of Defence, E-in-C's branch, Kashmir House, Rajaji Marg, New Delhi 110011, India

Note: This paper is part of the special topic, Flow and the Virus.
[a)]**Author to whom correspondence should be addressed:** agupta@mech.iitd.ac.in

ABSTRACT

Since the beginning of the COVID19 pandemic, there has been a lack of data to quantify the role played by breathing-out of pathogens in the spread of SARS-Cov-2 despite sufficient indication of its culpability. This work aims to establish the role of aerosol dispersion of SARS-Cov-2 virus and similar airborne pathogens on the spread of the disease in enclosed spaces. A steady-state fluid solver is used to simulate the air flow field, which is then used to compute the dispersion of SARS-Cov-2 and spatial probability distribution of infection inside two representative classrooms. In particular, the dependence of the turbulent diffusivity of the passive scalar on the air changes per hour and the number of inlet ducts has been given due consideration. By mimicking the presence of several humans in an enclosed space with a time-periodic inhalation–exhalation cycle, this study firmly establishes breathing as a major contributor in the spread of the pathogen, especially by super-spreaders. Second, a spatial gradient of pathogen concentration is established inside the domain, which strongly refutes the well-mixed theory. Furthermore, higher ventilation rates and proximity of the infected person to the inlet and exhaust vents play an important role in determining the spread of the pathogen. In the case of classrooms, a ventilation rate equivalent to 9 air changes or more is recommended. The simulations show that the "one-meter distance rule" between the occupants can significantly reduce the risk of spreading infection by a high-emitter.

I. INTRODUCTION

Human history is freighted with memories of several deadly outbreaks of diseases responsible for causing untold misery and suffering among the global population, leaving deep scars on the social and psychological well-being of the individuals as well as the society. SARS-Cov-2 brought those memories, buried in the pages of history, back after the outbreak that started in late 2019 from the Wuhan province of China.[1] The spread of the disease and devastation unleashed by it seemed uncontrollable and have caused 645×10^6 infections and 6.6×10^6 deaths[2] across the world as of November 2022. SARS-Cov-2 is transmitted to a susceptible person by respiratory droplets emitted by an infected person. A susceptible person can get infected by large droplet transmission to conjunctiva or mucus membrane, by self-inoculation through fomites or by inhalation of aerosols or microdroplets.[3–6] The droplets are emitted by various expiratory events, such as sneezing, coughing, breathing, talking, and singing. Other several highly pathogenic and infectious diseases, like H5N1, H1N1, and tuberculosis, are also transmitted via the respiratory route. The World Health Organization (WHO) has formulated that particles having diameter less than 5 μm are called droplet nuclei while particles having diameter greater than 5 μm are called droplets.[7] The guidelines issued by various governments, such as social distancing, six-foot rule, use of masks and sanitizers, and isolation of the infected person, assumed predominance of droplet transmission as the primary mode of SARS-Cov-2 infection. However, the rapid spread of SARS-Cov-2, especially in indoor spaces, has brought aerosol transmission of the virus in focus.

Several researchers starting from Wells[8] and Duguid[9] have studied size distribution, duration of carriage, mechanism of formation, and spread of droplets in an environment. Droplets are formed in different areas of the respiratory tract with their size and viral load depending upon the site of origin.[10] Papineni and Rosenthal[11] showed that 80%–90% of particles exhaled from human expiratory activities are smaller than 1 μm in diameter. Morawska *et al.*[12] showed that the different physiological processes have specific size distribution modes associated with them. They reported that a large number of particles

were produced in modes having diameters below 0.8 μm at an average concentration of 0.75 cm^{-3}. This result has an important implication for the present study as it demonstrates that many particles are emitted in the form of aerosols. The size of these particles is small enough to model them as a passive scalar as they do not affect the flow field and large enough for the particles to be unaffected by Brownian motion. Furthermore, the short-timescale of evaporation justifies modeling the spread of the pathogen bearing droplets as aerosol with larger droplets settling under gravitational effect within 1 s.[12]

Ambient conditions, such as high temperature and low relative humidity, have an important bearing on the size and aerosolization of the exhaled droplets.[13,14] Higher wind velocities increase the distance traveled by the droplets before settling under gravity.[15–17] Expiratory velocity also plays a major role with large expelled droplets being carried to longer distances with increased exhalation velocities.[13]

Out of all exhalation events, the role of coughing and sneezing in transmission of disease in different scenarios has been analyzed in great detail.[10,15–25] The inferences from various studies are that the six-foot rule may not be sufficient, whereas air-conditioning and ventilation help in diluting the pathogen concentration but increase its spread, while poorly designed heating, ventilation, and air-conditioning (HVAC) systems may worsen the situation.

However, the rapid spread of SARS-Cov-2 has established aerosol transport as a major cause for its spread. Doremalen *et al.*[26] reported that SARS-Cov-2 remained viable as aerosol during three-hour duration of the experiment with half-life of 1.1–1.2 h in air, implying the possibility of aerosol transmission resulting in its transmission to a larger area and distances infecting many persons. This silent transmission of SARS-CoV2 especially by asymptomatic subjects has been the key mechanism for spread of the virus. An experimental study in a Swedish hospital detected active SARS-Cov-2 virus from air in COVID-19 patients' rooms and adjoining ante-rooms, establishing transmission through aerosols.[27] A numerical evaluation of SARS-Cov-2 spread in a single-family house with patient under home quarantine with standard ventilation showed that aerosol transmission remains a prominent risk.[28] Some other researchers have also studied the aerosol transport and inhalation of these respiratory aerosols.[29–31]

Yan *et al.*[32] posited that the detection of culturable virus in fine aerosols in the absence of cough implies the presence of other mechanisms like breathing and talking for aerosol generation. Many researchers have concluded that normal breathing by an asymptomatic person can produce higher aerosol numbers during the day than coughing as it involves higher flow rates.[11,14,33–35] Zhang *et al.*[36] reported that the wearing of face masks has been an effective strategy compared to social distancing in controlling the spread of the disease, implying that airborne transmission through smaller particles represents the dominant route in spread of SARS-Cov-2. The smaller particles can persist in the environment for a longer duration, penetrating into the lower tract of the lungs causing respiratory infection of lower lungs, which is more dangerous.[10,37–39] Furthermore, smaller droplets ($\sim$2 μm) are two or more orders of magnitude more infectious than larger droplets ($>$ 10 μm).[39] Asadi *et al.*[37] reported that a small fraction of individuals known as superemitters consistently emit an order of magnitude more particles than the average emitter and are disproportionately responsible for the spread of infection. These observations are particularly important in view of the closed environment with multiple occupancy such as offices, classrooms, and auditoriums.

From the preceding paragraphs, it is evident that dispersion of aerosols emitted during breathing plays a prominent role in the spread of any airborne disease. However, an analysis on the role of breathing in the spread of the pathogen in enclosed spaces is severely lacking. Also, many studies have been limited in scope as the number of occupants considered was either one or two or a very small group of less than 10 persons. In such a scenario, the analysis is compromised when decisions are to be made for a room with a considerably large number of occupants. Furthermore, some analyses have assumed a well-mixed scenario in indoor spaces, e.g., Bazant and Bush[6] and Buonanno *et al.*[40] The well-mixed model assumes a constant concentration of the pathogen inside the enclosed space and an equal risk of infection irrespective of the distance from the source. On the contrary, the risk of infection must have an inverse dependence on the distance from the source. In such a scenario, to prescribe safety guidelines and suggest measures to mitigate the effect of the pathogen using the well-mixed approach become questionable. Therefore, we have performed computational modeling of SARS-Cov-2 aerosol dispersion in two typical classrooms to establish the role of breathing in the spread of the virus in indoor spaces. Using the layout for standard classrooms with occupancy and ventilation provisions, the spread of the aerosol generated due to breathing and the risk posed by an infected (symptomatic or asymptomatic) person to other occupants have been quantified. While the analysis presented was initiated in the backdrop of the spread of SARS-Cov-2 pandemic, the results presented are also applicable to the dispersion of similar airborne pathogens.

II. MATERIAL AND METHODS

To model the effect of breathing by an infected person in a large domain having large number of occupants, such as in classroom setting, a steady-state solver is used to obtain the air flow field. Furthermore, the length scale of the pathogen is sufficiently small due to which it can be assumed that its effect on the flow field is negligible. The air flow inside an air-conditioned space is turbulent. Hanzawa *et al.*[41] reported that the turbulence intensity varied from 10% to 60% at the head level and 10%–70% at the ankle level. Xia *et al.*[42] prescribed a range of 25%–40% for turbulent intensity inside the indoor environment. The three-dimensional fluid flow is simulated using the widely followed two-equation turbulence models (k–ε, RNG k–ε, and k–ω). For brevity, only the standard equations for the k–ε model are given in Appendix A.

The average volume of air inhaled or exhaled by an adult is 0.5 m^3/h.[43] Breathing leads to generation of many small droplets, and time taken for their evaporation is less than 0.8 s.[12] Therefore, droplets generated during breathing can be modeled as aerosols (the concentration of which is represented using a passive scalar ϕ) in a flow field with a source-term imitating the human breathing cycle. The evolution of transport of the passive scalar inside the domain can be observed for a duration of interest to assess the spread of the pathogen. A conserved passive scalar field can be decomposed into its mean and a fluctuating component,[44]

$$\phi(x,t) = \langle \phi(x,t) \rangle + \phi'(x,t), \tag{1}$$

where $\phi(x,t)$, $\langle \phi(x,t) \rangle$, and $\phi'(x,t)$ are the concentration, mean, and the fluctuating component of the passive scalar, respectively.

TABLE I. Estimation of quanta emission rate for value of infectious dose of $c_i = 0.02$.

Number	Reference	RNA copies/hour in exhaled breath	Quanta emission rate
1	Ma *et al.*[48]	5×10^4–5×10^6	1000–100 000
2	Malik *et al.*[49]	3.2×10^3–1.32×10^6	64–26 400
3[a]	Buonanno *et al.*[40]	1.2×10^2–1.2×10^5 (Corresponding to 10^8–10^{11} RNA copies in sputum)	2.3–2332

[a]Calculated as per the procedure mentioned in Ref. 40.

TABLE II. Emission rates (in quanta per hour) for different levels of emitters considered in this study.

	Low emitter	Medium emitter	High emitter	Superemitter
Emission rates (in quanta/h)	6.4	64	640	≥6400

The conservation equation for the $\Phi(x, t)$ can be written as

$$\frac{\partial \phi}{\partial t} + \nabla \cdot (\vec{U}\phi) = \Gamma \nabla^2 \phi, \tag{2}$$

where $\vec{U}$ is the fluid velocity field and Γ is the diffusivity of the passive scalar.

The velocity in a turbulent field can be decomposed into its mean and fluctuating component using Reynolds decomposition,

$$\vec{U}(x, t) = \left\langle \vec{U}(x, t) \right\rangle + \vec{u}(x, t), \tag{3}$$

where $\vec{U}(x, t) = \text{Velocity field}$, $\left\langle \vec{U}(x, t) \right\rangle = \text{ensemble} - \text{averaged velocity field}$, and $\vec{u}(x, t) = \text{fluctuation part}$.

Taking time average of Eq. (2), we have

$$\frac{\partial \langle \phi \rangle}{\partial t} + \langle \vec{U} \rangle \cdot \nabla \langle \phi \rangle = \nabla \cdot \left(\Gamma \nabla \langle \phi \rangle - \left\langle \vec{u} \phi' \right\rangle \right).$$

In this equation, the scalar fluxes $\left\langle \vec{u} \phi' \right\rangle$ play a role analogous to the Reynold stresses. The equation can be represented as

$$\frac{\partial \langle \phi \rangle}{\partial t} + \langle \vec{U} \rangle \cdot \nabla \langle \phi \rangle = \nabla \cdot (\Gamma_{\text{eff}} \nabla \langle \phi \rangle), \tag{4}$$

where Γ_{eff} is sum of molecular and turbulent diffusivities.

The time average of a source term can be added to the above equation to model the passive scalar for aerosols generated. To solve the discretized equation, the estimation of breathing rate, volume expired in a breath, concentration, or quanta of the pathogen in the suspended aerosols and order of effective or eddy diffusivity in the turbulent flow are required.

It has been posited that SARS-Cov-2 is an order of magnitude more infectious than SARS CoV-1.[6] However, there are no definite studies available for the level of infectious dose of SARS-Cov-2. Based on modeling, animal studies and experience of SARS-Cov-2 and other similar diseases, the current estimates of number of virions needed to cause an infection in the case of SARS-Cov-2 have been reported to be in the range of 10–1000.[40,43,45–47] Generally, an infectious dose is represented in terms of quanta or HID_{50}. A quanta is defined as the dose of airborne droplet nuclei required to cause infection in 63% of the susceptible population,[40] while HID_{50} is defined as the minimum infectious dose required to cause infection in 50% of the population.[39] As the quanta is more prevalent in use, it has been chosen to define the infectious dose in this study.

As per experiments carried out by Ma *et al.*,[48] SARS-Cov-2 levels in the exhaled breath could reach $10^5 - 10^7$ RNA copies/m^3. The breath emission rate is highest during the early stages of the infection, thus highlighting the role of asymptomatic patients in spread of the virus. Malik *et al.*[49] conducted several experiments showing that the viral load in pharyngeal mucus and exhaled breath have no correlation. The mean viral load from the swab taken from mucus was 7.97×10^6 RNA copies, whereas from exhaled breath, it was $2.47 \times 10^3 (7.19 \times 10^1 - 2.94 \times 10^4)$ RNA copies for twenty instances of exhaling. Buonanno *et al.*[40] mentioned a viral load of $10^8 - 10^{11}$ RNA copies/ml in the sputum based on various estimates.[6,43,45,46,50–52] The value of index for infectious dose in the present study is taken as $c_i = 0.02$, which is similar to that taken by Buonanno *et al.*[40] Based on these studies, the SARS-Cov-2 RNA copies emitted per hour and quanta emission rate where $c_i = 0.02$ for a breathing rate of 0.5 m^3/h are given in Table I.

As the viral load in pharyngeal mucus and exhaled breath has no correlation,[49] a quanta emission rate of 6.4–6.4 $\times 10^3$ is considered in the present study corresponding to a range from 10^2 to 10^5 RNA copies/hour of exhaled breath. The quanta emission rates considered in this study are categorized in Table II. Both high and superemitters can be categorized as superspreaders.

As the pathogen is being modeled as a passive scalar in a turbulent flow, eddy or turbulent diffusivity, Γ, is calculated using Eq. (1),[53]

$$\Gamma = \frac{0.824\, Q}{(VN^2)^{1/3}}, \tag{5}$$

where Q is the ventilation rate (or air changes per hour), V is the volume of the room, and N is the number of supply air inlets. The open-source package OpenFOAM is used to perform fluid flow and aerosol transport calculations. The package has an extensive library of computational fluid dynamics (CFD) solvers based on various models for several flow situations. To decide the turbulence model to be used and to validate the solver, the flow in a three-dimensional lid-driven cavity is simulated and compared with published experimental results. The problem of fluid flow due to an induced shearing of the top surface

has been used to benchmark the solver as complex fluid phenomena are observed in it despite its simple geometry.

The flow in a three-dimensional lid-driven cavity case is simulated for $Re = U_w H/\upsilon = 10\,000$ (where U_w is the wall velocity, H is the side-length of the cubic cavity, and υ is the kinematic viscosity of the fluid) using different turbulence models in OpenFOAM. The results are compared with the experimental results obtained by Prasad and Koseff[54] for flow of water in a belt driven cavity of square cross section. A non-uniform $128 \times 128 \times 128$ mesh was employed. The second-order upwind scheme was used for discretization of the Navier-Stokes equation. The result obtained is compared graphically with published data in Fig. 1.

The results obtained by Shankar and Deshpande using direct numerical simulation (DNS)[55] have also been plotted for comparison. Except slight deviation near the walls, the flow phenomena are captured well by k–ϵ and RNG k–ϵ models and their performance is better than that of the k–ω model. Shanker and Deshpande[55] have also noted that the results obtained by DNS compared quite well for the streamwise components over the whole range; the downward components have mismatch of peaks of almost 25% near the downstream sidewall. Similar deviation with experimental results has also been noted in several other studies[56–60] using different techniques, such as DNS and LES. The results obtained by using k–ϵ and RNG k–ϵ models are almost similar, but the time taken for convergence is less in the case of k–ϵ. The results were also verified using two other commercial packages (namely COMSOL Multiphysics and ANSYS Fluent) and were found to be in good agreement with OpenFOAM. Hence, the k–ϵ model was selected to obtain the air flow field in all scenarios presented from here onward.

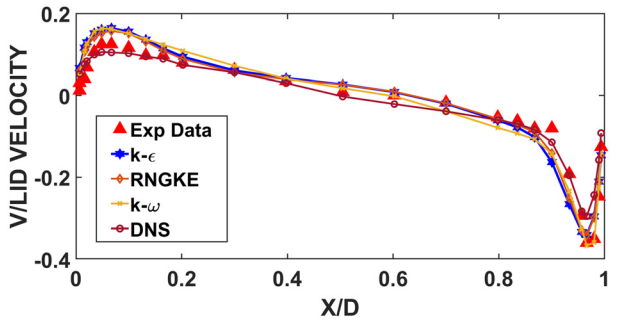

(a)

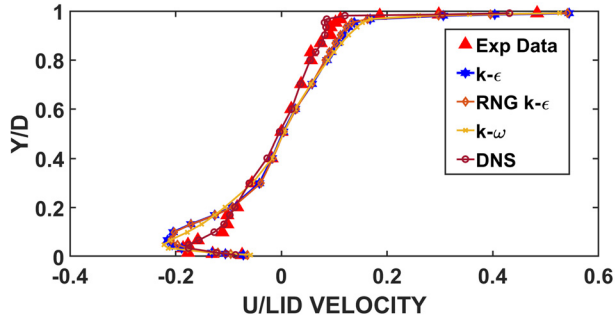

(b)

FIG. 1. A comparison of the (a) Y-component of normalized mean velocity with centerline along the X direction and (b) X-component of normalized mean velocity with centerline along the Y direction against published data.

III. RESULTS

The design case of a typical lecture classroom at IIT Delhi, which has an occupancy of 60 attendees, is considered first. The domain for the problem is sufficiently large and has a reasonably high occupancy to evaluate the effect of breathing by an asymptomatic occupant. The three-dimensional schematic of the lecture hall recreated using the open-source package Blender is shown in Fig. 2. Human mannequins, 60 in number, in a seated position with standard furniture, i.e., tables and chairs, are placed in this domain. The dimensions of the lecture hall are $9 \times 7.5 \times 3.2$ m^3. The supply of air to the room is through the air diffusers placed on the ceiling. A total of 8 supply air diffusers with square cross section of size 150 mm have been provided. Four return air outlets of rectangular cross section and size 300×150 mm^2 at a height of 25 cm from the floor level in side walls have also been included. The inlet air velocity is 2 m/s for a ventilation rate equivalent to 6 air changes per hour (ACH). The turbulence intensity has been assumed to be 22.4% and Reynolds number, $Re = 19\,200$ (where $Re = UH/\upsilon$, U is the mean fluid velocity through inlet diffuser, H is the hydraulic depth of the inlet diffuser, and υ is the kinematic velocity of the fluid). Boundary conditions for velocity are taken as zero gradient at outlets, no slip at stationary surfaces, and prescribed value at inlet. Boundary conditions for pressure are taken as zero gradient at inlet and at surfaces and prescribed value at outlets.

The drawings are exported to OpenFOAM and meshed as shown in Fig. 3. The hexahedral cells are used for meshing. The domain was discretized using three different resolutions for reaching grid independent solutions, namely, 15.02×10^6, 22.72×10^6, and 33.1×10^6 cells. It is found that the maximum relative L_2 norm for velocity components, when measured relative to the finest resolution, decreases from 2% to less than 0.1% when the number of cells is increased from 15.02×10^6 to 22.72×10^6. Hence, the latter resolution is chosen for conducting all the simulations as sufficient accuracy is considered to have been achieved. Due to the large number of cells, the domain is subdivided into sub-zones and run on twelve processors in parallel to limit the time taken for each simulation.

A. Passive scalar transport of pathogen

After obtaining the steady-state solution of the flow field, the transport of pathogen as a passive scalar in the classroom is simulated. Following are the assumptions made for these simulations:

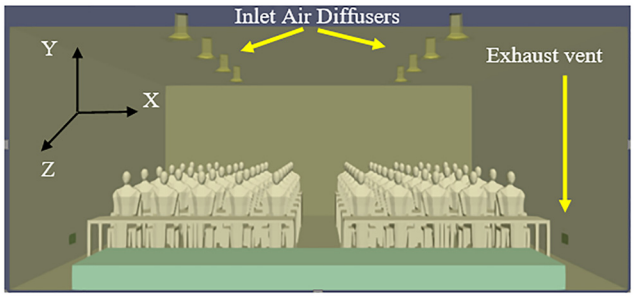

FIG. 2. A recreated schematic of the three-dimensional representation of a typical lecture room of 60 occupants at IIT Delhi.

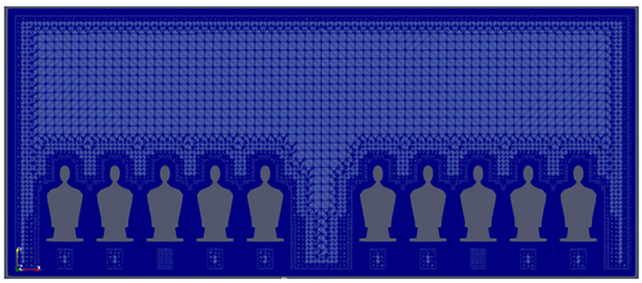

(a)

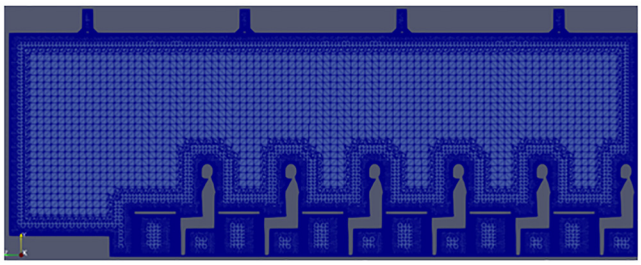

(b)

FIG. 3. Mesh of a classroom with 60 occupants. (a) Front view (XY plane). (b) Side view (YZ plane).

(a) Turbulent diffusion coefficient, Γ, is assumed to be constant and isotropic throughout the spatial and temporal domain.
(b) All the occupants are assumed to have similar physical dimensions and seated equidistant from each other. The seating arrangement is shown in Fig. 2.
(c) All the occupants have the same breathing volumetric flow of 0.5 m^3/h and a breathing rate of 15 breaths per minute.[61,62]
(d) A square wave of time period 4 s is assumed to imitate the breathing pattern with equal duration of exhalation and inhalation (i.e., 2 s each). During exhalation, it is assumed that the pathogen is emitted at a uniform rate.
(e) The pathogen is not re-inhaled by the infected person during the inhalation phase to model the worst-case scenario where all the pathogens exhaled by the infected person into the domain are available for spreading the infection.
(f) The movement of the occupants is not considered.
(g) All the fresh air is supplied from the supply diffusers, and no infiltration of the air is present from any other source.
(h) All the air escapes from the exhaust vents or the door provided.
(i) There is no pathogen infiltration from the fresh air supplied to the room.
(j) Angle of breath exhalation is taken as given by Gupta *et al.*[63]
(k) It is assumed that the room is at a constant temperature.

Other input parameters for performing simulations for this room are given in Table III. Using these parameters, the turbulent diffusivity coefficient calculated using Eq. (5) is 0.012 36 m^2/s.

We consider that the location of the asymptomatically infected person is shown in Fig. 4. The duration of occupancy has been considered to be one hour. It is intuitively felt that after some time, the concentration of the passive scalar in the domain will spatially stabilize. To test the premise, the variation in a rate of concentration changes with time at various points in a plane at the nose level of the occupants i.e., 1.15 m from ground level, has been calculated and is depicted in Fig. 5.

TABLE III. Input parameters for the simulation of pathogen transport in a room with 60 occupants.

Parameter	Description	Value based on measurements
Q	Rate of supply of air in the room	0.36 m^3/s
V	Volume of the room	216 m^3
N	Number of supply air diffusers	8

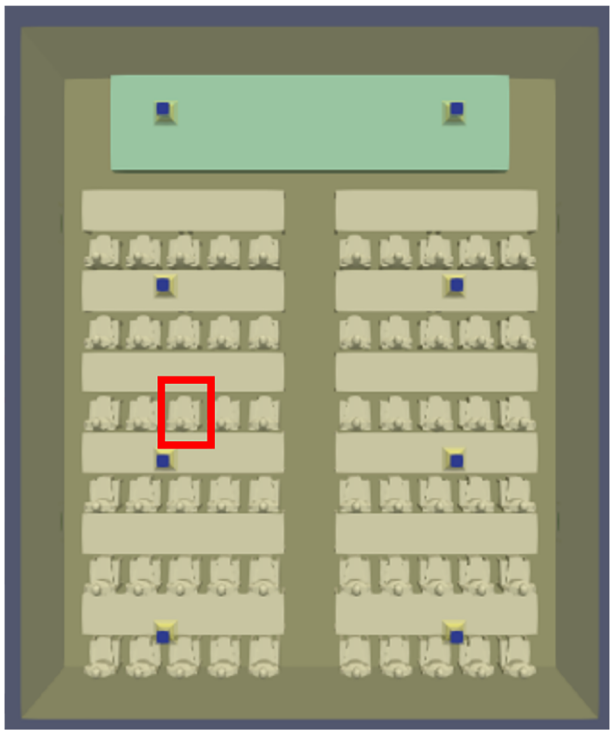

FIG. 4. Location of infected person shown in red rectangular box.

It can be seen from Fig. 5 that the slope of concentration change of pathogen reduces by an order of magnitude with time from 300 to 1800 s, implying that the concentration of the pathogens stabilizes spatially after some time i.e., the distance from the source where there would be higher chances of infection can be clearly demarcated.

B. Effect of changing ventilation rate or air changes per hour (ACH)

The ventilation rate is an indicator of the rate at which fresh air is brought into an indoor space. Typically, it is represented by air

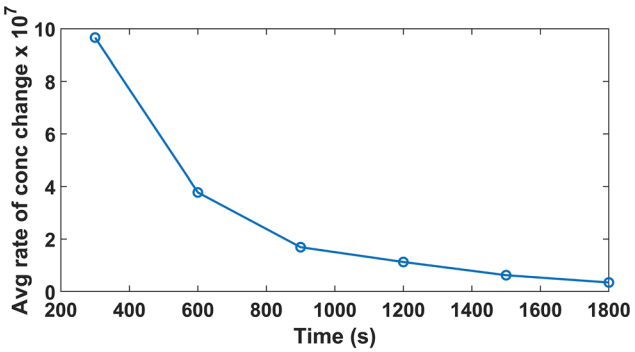

FIG. 5. Variation of an average rate of concentration change with time.

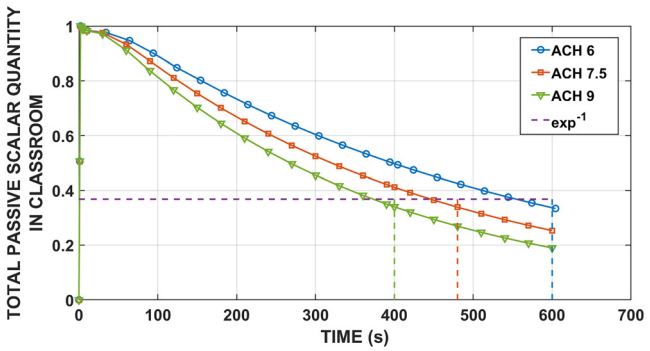

FIG. 7. Variation of passive scalar injected for a duration of 2 s.

changes per hour (ACH). In this work, the ventilation rate is varied by changing the air supply rate from the supply air diffusers. The various parameters for different ventilation rates are given in Table IV. The contours of velocity magnitude obtained for an ACH of 6 for the classroom of 60 occupants are shown in Fig. 6. This figure shows the flow contours at the YZ plane at X = 1.875 m and XY plane at Z = 2.25 m, where the coordinates are measured with respect to the geometric center of the domain. Air velocities at different heights are found to be less than 0.5 m/s except for the locations near to the supply and exhaust ducts. The section in the XY plane at Z = 2.25 m intersects the location of center of exhaust duct in the bottom portion of the side walls, whereas the section in YZ plane at X = 1.875 m intersects the center of the supply air ducts.

The effect of ACH on residence time of the pathogen inside the classroom was studied by simulating a single pulse of breath by an infected person positioned as shown in Fig. 4. The change in total quantity of the passive scalar with time inside the classroom for all the cases was calculated.

It can be inferred from Fig. 7 that the total quantity of passive scalar inside the classroom decays exponentially and reduces by approximately 63% in a time equivalent to one change of air in the classroom. Thus, the time constant, τ, for decay of total quantity of pathogen inside the classroom is inversely proportional to the ACH, i.e., $\tau \propto \frac{1}{ACH}$ or $Q_p = Ae^{\frac{-Bt}{ACH}}$, where Q_p is the quantity of passive scalar inside the classroom after time t, and A and B are constants.

As the air change for a naturally ventilated space is 0.5/h,[40] an important conclusion for naturally ventilated spaces where doors are kept open is that it takes approximately two hours for the pathogen concentration to reduce by 63% even after the infected person has left the space. Also, increasing the ventilation rate inside the enclosed space

TABLE IV. Inlet air velocity and ventilation rate for a room with occupancy of 60 people.

Case	Description	Inlet air velocity (m/s)	Re	Γ (m²/s)	Ventilation rate (ACH)
1	Case I	2	19 200	0.0124	6
2	Case II	2.5	24 000	0.0155	7.5
3	Case III	3	28 800	0.0185	9

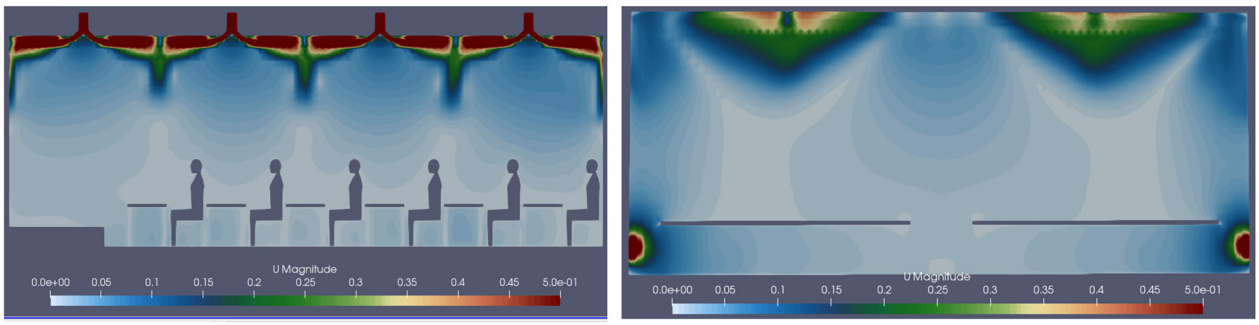

(a) (b)

FIG. 6. Velocity magnitude contours for the classroom with 60 occupants and having a ventilation rate of 6 ACH. The velocity magnitude is shown at two sections corresponding to (a) YZ plane at X = 1.875 m and (b) XY plane at Z = 2.25 m.

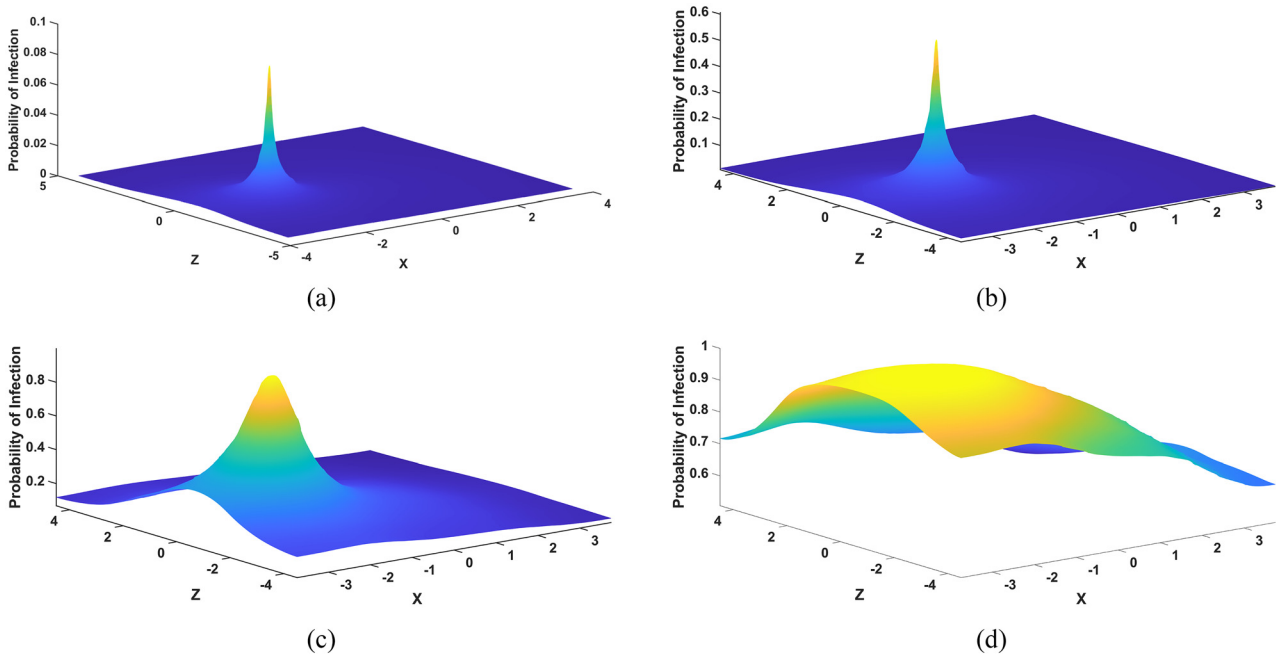

FIG. 8. Probability magnitude for different type of emitters on XZ plane at Y = 1.15 m (nose level) for ventilation rate of ACH = 6. Dimensions are in meter. (a) Low emitter. (b) Medium emitter. (c) High emitter. (d) Superemitter.

reduces the residence time of the pathogen. However, increasing ventilation rate has diminishing returns with respect to the residence time.

The results of the simulation for different ventilation rates are listed in Table V. The probability of infection is calculated by total quanta, q, which is inhaled by a person in an hour at a particular location. The probability of infection is calculated using $P = 1 - e^{-q}$, where P is the probability of infection and q is the quanta of pathogen inhaled. It can be observed from these data and that is shown in Fig. 8 that there is very low risk for the spread of the pathogen from a low and medium emitter. For high emitters, there is almost 50% expectation of the pathogen within a radial zone of 1 m. The contour of probability of infection with distance is shown in Fig. 9 for a high emitter. In the case of superemitters, it can be said that no one is safe from the pathogen. Even at a distance of 6 m, there is a high risk of infection (Table V).

Thus, it is firmly established from the results that aerosol dispersion by breathing is a major risk in spread of the virus. The same assertion is found in study by Picard *et al.*[28] for a person under home quarantine and the experimental investigation carried by Sousa *et al.*[27] In the case of high emitters, a distance of one meter between the occupants reduces the risk to almost 50% and, hence, can be adopted as a strategy to devise seating plans in the case of an apprehension of the spread of a pathogen. Arumuru *et al.*[64] while doing the experimental study to analyze breathing have shown that reach of the breath is up to 4 ft or 1.2 m, which is in consonance with the one-meter distance suggested in this study as safe distance in the case of an asymptomatic person, who is neither coughing nor sneezing.

Another way of analyzing these data is to find out the number of susceptible persons for the present seating arrangement in the classroom. This may, however, vary with the type of seating arrangement but can provide an understanding of the effectiveness of the ventilation rate.

It is evident from Fig. 9 that the passive scalar or pathogen spread is highly stratified even after reaching a steady state inside the room contrary to the assumption in the well-mixed model. The distance from the infected person is highly crucial in reducing the chances of infection. Therefore, it is important to have a seating arrangement maintaining a distance of at least one meter between the occupants to reduce chances of infection. The well-mixed model may provide an estimate of the number of susceptible persons inside an enclosed space but may not give the minimum distance required to reduce the chances of spread of infection and cannot bring out the stratification of pathogen spread inside the indoor space, which has been clearly brought in the present model.

Furthermore, superspreaders have been blamed for the large scale spread of SARS-Cov-2. These results clearly highlight the role of superspreaders (classified as high and superemitters in the present study) in the spread of SARS-Cov-2. Not only the reach or distance to which the pathogen spreads but also the number of occupants susceptible to infection is disproportionately high in the case of superspreaders.

The role of high ventilation rate in reducing the spread of the pathogen is crucial. It is observed that increase in ventilation rate not only decreases the residence time of virus and radial zone of high infectiousness, it also reduces the number of susceptible people in the enclosed space. This aspect is crucial in the case of breakdown of another pandemic. In such a scenario, the easiest method to mitigate the spread of virus is to increase the ventilation rate inside the enclosed space. The finding is supported by Noakes *et al.*[65] They claimed that

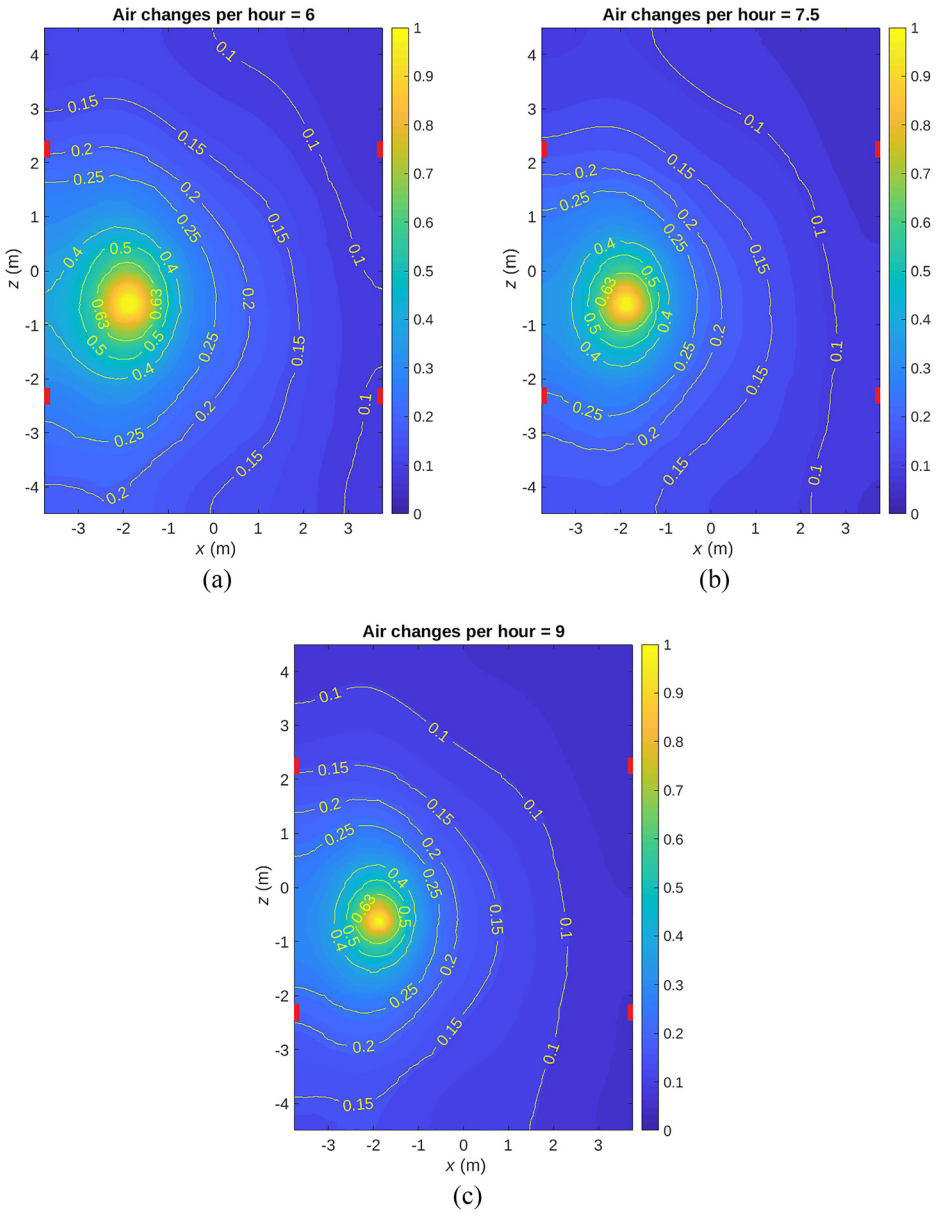

FIG. 9. Contour of probability of infection by high emitter for varying ventilation rates on XZ plane at Y = 1.15 m (nose level). Red rectangle indicates the position of the exhaust duct on the side walls. (a) Case I: ACH = 6. (b) Case II: ACH = 7.5. (c) Case III: ACH = 9.

high ventilation rates may remove the potential of epidemic altogether. However, this may not be true as increasing the ventilation rate does not drastically reduce the infection probability. As is evident from Table VI, in the case of high emitters, with the increase in the ventilation rate from 6 ACH to 9 ACH (an increase in 50%), for 63% or higher probability of infection, the maximum range of infection or minimum safe distance from the infected person reduces from 0.8 to 0.52 m i.e., a reduction of 35%. Similarly, from Table VI, the number of susceptible persons for present seating arrangement decreases from 13 to 10, i.e., a reduction of 23%. As the ventilation rate cannot be increased beyond a certain limit owing to HVAC system capacity and human comfort requirements, it is not possible to remove the potential of the epidemic altogether. Still every life saved is worth the effort. ASHRAE in guidance for re-opening of schools emphasized on providing a good supply of air to mitigate the risk of infection.[66] According to the ASHRAE standard 62.1–2010,[66] ventilation rates equivalent to at least 9 air changes or more per hour can be provided in the lecture halls. The recommendation must be used in the case of a pandemic having propensity to spread by aerosol dispersion.

C. Effect of position of asymptomatic person

To gauge the effect of position of the infected person on the spread of infection, three cases with different positions of the infected

TABLE V. Probability of infection vs the maximum distance from the source of infection at the plane of nose level for different ventilation rates.

Emitter level→	Low emitter			Medium emitter			High emitter			Superemitter		
	Air changes per hour											
Probability of infection ↓	6	7.5	9	6	7.5	9	6	7.5	9	6	7.5	9
	Maximum distance (m)											
≥ 63%	Negligible risk of infection			⋯	⋯	⋯	0.8	0.6	0.52	6.53	5.79	5.35
≥ 50%				0.04	0.03	⋯	1.19	0.95	0.75	7.63	6.89	6.43
≥ 25%				0.22	0.12	0.1	2.96	2.58	2.24	Whole classroom		
≥ 10%				0.77	0.59	0.48	6.15	5.63	5.14			

TABLE VI. Number of susceptible persons in the classroom for assumed seating arrangement for different ventilation rates.

	Susceptible persons		
Category	(ACH 6.0)	(ACH 7.5)	(ACH 9)
Low emitter	0	0	0
Medium emitter	2	1	1
High emitter	13	12	10
Superemitter	50	48	45

person were simulated for the ventilation rate equivalent to 6 ACH. The position of the infected person in each case is shown in Fig. 10.

It can be observed from Fig. 11 and Table VII that the position of the infected person affects the maximum distance of spread of infection. In case V, the maximum distance for high probability of infection is considerably higher than the other locations. This is due to the fact that in this position, the distance of the infected person from the exhaust duct is large as compared to other locations and air in this location pushes the pathogen toward the rear wall leading to an increase in the concentration of the pathogen over a larger area. In case IV, the spread of the pathogen reduces as it is nearest to the exhaust duct compared to other locations. However, in all the three cases, a distance of one meter is enough to protect the occupants from the pathogen.

D. Effect of position of exhaust ducts

To evaluate the effect of position of the exhaust duct, another case was simulated with exhaust ducts of similar area but provided on the ceiling for ventilation rate equivalent to 6 air changes per hour. In case I shown previously, Fig. 4, exhaust vents were considered on the side walls. In this new configuration, the position of the ceiling exhaust ducts is 30 cm away from the side walls (case VI) as shown in Fig. 12.

It was speculated that providing ceiling exhaust may help in lifting the pathogen out of the breathing zone toward the ceiling. However, results in Fig. 13 and Table VIII indicate that it does not serve this purpose. Rather, in this configuration, the reach of the pathogen in the room increases further when considering the case of a superemitter. This can be explained by the fact that the inertia of the supply air from the ceiling enables the pathogen to be swept downward toward the floor. After a short time interval, these pathogens are again lifted up toward the ducts provided in the ceiling, thereby increasing their dispersion and exposure to occupants.

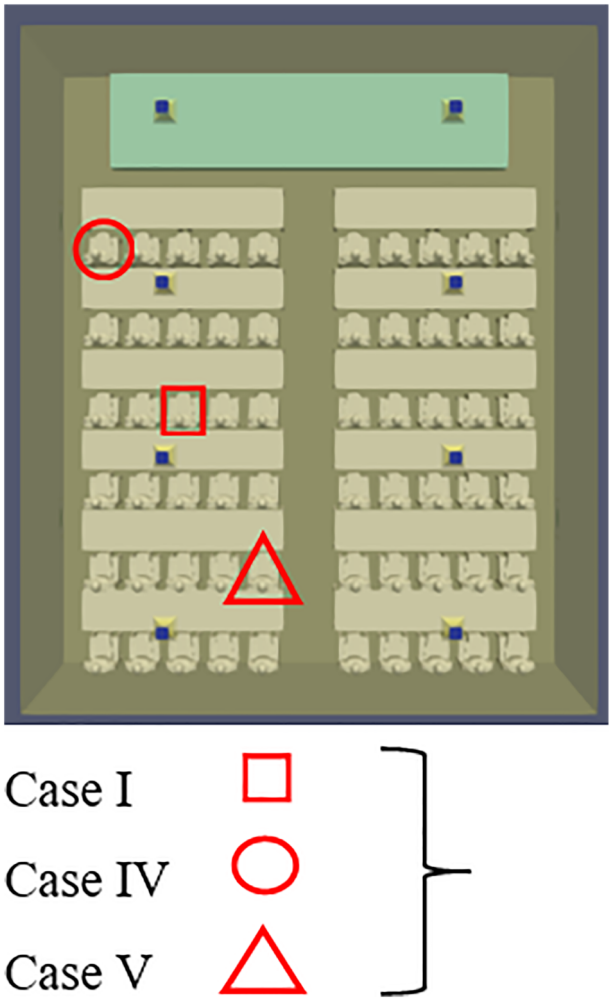

FIG. 10. Different positions of the infected person simulated for ACH = 6.

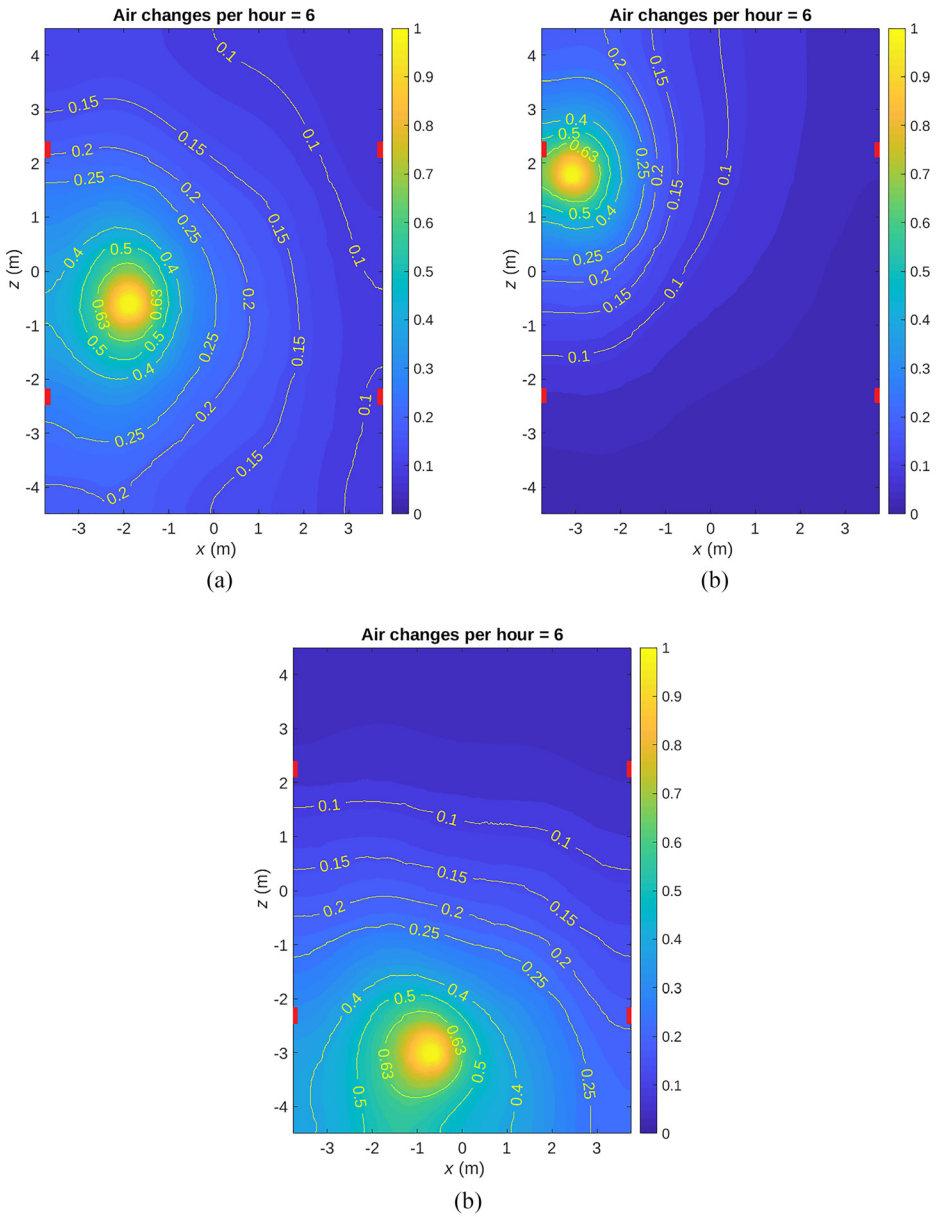

FIG. 11. Contours of probability of infection for three different positions of the infected person with the same ventilation rate in the case of a high emitter. (a) Case I. (b) Case IV. (c) Case V.

IV. DISPERSION ANALYSIS OF A LARGER ROOM

An analysis of the spread of the pathogen is carried out for a larger lecture room at IIT Delhi. This room, whose layout is shown in Fig. 14, has a seating capacity of 168. The velocity of the air from the inlet supply ducts was measured using a hot wire anemometer, and the ventilation rate was calculated, which was equivalent to 9 air changes per hour. There are ten supply ducts in the ceiling and ten exhaust ducts in the ceiling along the side walls. The other input variables for performing the fluid flow and dispersion calculations are listed in Table IX. The number of cells in the domain were 51.12×10^6, and the mesh is shown in Fig. 15.

The computational modeling of the dispersion of the pathogen was conducted for two locations of the infected person (source) as shown in Fig. 16. It must be noted that the flow field remains the same in both these cases, and only the passive scalar transport of the pathogen is simulated separately. The simulation is performed for one hour, which is typically the duration of a lecture.

Table X provides the probability of infection as a function of distance for the two different locations assumed by an infected person. It can be observed from Table X that irrespective of the position of the infected emitter, the risk of infection in the case of low and medium emitters is very low. However, for a high emitter, one meter between

TABLE VII. Probability vs maximum distance of infection for different seating arrangements for a ventilation rate of 6 ACH. WC stands for "whole classroom."

Emitter level →	Low emitter			Medium emitter			High emitter			Superemitter		
	I	IV	V	I	IV	V	I	IV	V	I	IV	V
Probability of infection ↓	Maximum distance (m)											
≥63%	Negligible risk of infection			⋯	0.07	0.04	0.8	0.66	1.08	6.53	4.53	5.73
≥50%				0.04	0.10	0.07	1.19	0.80	2.09	7.63	5.90	6.53
≥25%				0.22	0.21	0.17	2.96	1.90	3.82	WC	7.64	WC
≥10%	⋯	0.07	0.06	0.77	0.74	0.98	6.15	4.29	5.61	WC	WC	WC

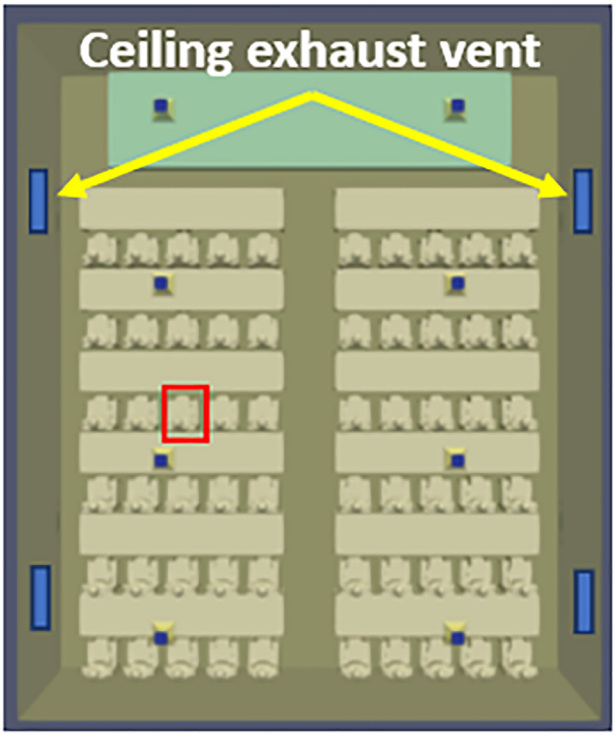

FIG. 12. Position of the ceiling exhaust ducts for case VI.

the occupants can substantially reduce the risk of infection. Tables X and XI show that a superemitter can infect about 50% of the occupants seated up to 10 m distance. In case A, the emitter is placed directly in front of the supply air duct, whereas in case B this person is placed in the back row far away from the supply air duct. From Fig. 17 and Table X, it can be observed that for a high emitter, the distance at which a high probability of infection is attained (i.e., ≥50%) is significantly increased in case B. However, the dispersion of the pathogen is higher in case A when compared with case B as can be observed by an increase in the distance for a low probability of infection (10% or higher). This is because the pathogen is being carried away to larger distances rapidly for the student in case A as compared to case B. In the case of a superemitter, the presence of the infected occupant directly in front of the inlet supply duct results in increased spread of the pathogen and a high probability of spread of the infection.

In the case of this lecture room, which has larger area and greater number of occupants as compared to the earlier case of a room with 60 occupants, the inferences are similar. That is, the risk posed by low and medium emitters is insignificant, a separation of one meter will reduce the risk of infection by almost 50% for high emitters and no strategy except masking is effective in the case of a superemitter.

V. CONCLUSIONS

This study primarily focused on dispersion of SARS-Cov-2 and similar airborne diseases in an enclosed space with many occupants. The simulations were performed for two standard classrooms at IIT Delhi. The $k-\epsilon$ model was used for obtaining the fluid flow field, and the transport equation of the pathogen was solved assuming pathogen to be a passive scalar. Various scenarios were simulated. The results of these simulations firmly established the role of breathing in the spread of SARS-Cov-2 virus. An asymptomatic patient who is a low emitter does not pose much risk. However, no strategy can mitigate the risk posed by a superemitter except for masking.

The study also underlines the importance of proper ventilation. It was shown that the residence time of the aerosol reduces considerably with an increase in the ventilation rate. For the seating plan considered in this study, the number of susceptible persons reduces on increasing the ventilation rate. The same may be true for any other type of seating plan if proper distance is maintained between the occupants. Conversely, in naturally ventilated spaces, such as schools or universities where ventilation rate is low, the pathogen can remain present for hours even after the room has been vacated by the infected person due to an increase in the residence time of the pathogen. Thus, it is recommended to make provisions for increasing the ventilation rate to reduce the risks associated with spreading of the infection. The highest possible ventilation rate, keeping in mind comfort and HVAC system capacity, must be used in a pandemic. In the case of classrooms, a ventilation rate equivalent to 9 air changes or more is recommended. Furthermore, these findings bring out the importance of keeping ventilation systems working for extended durations after closing hours to minimize the concentration of pathogen and contaminants in the building space.

The placement of exhaust duct also plays a crucial role in mitigating the spread of the pathogen inside the classroom. It was shown that when the supply air inlet is placed at the ceiling, it is beneficial to have

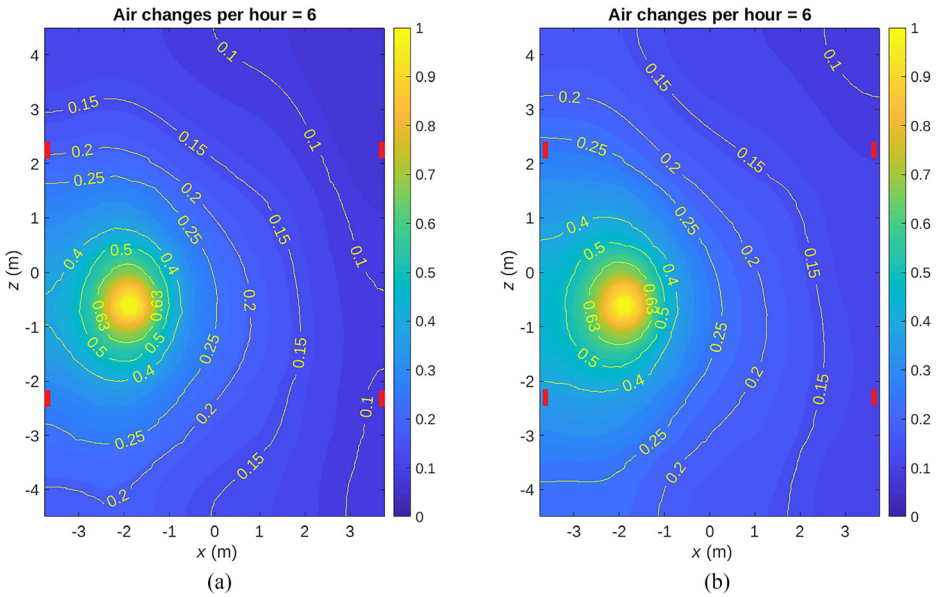

FIG. 13. Probability of spread of infection with different position of exhaust ducts with similar ventilation rate in the case of a high emitter. (a) Case I. (b) Case VI.

TABLE VIII. Comparison of probability of infection with maximum distance for different positions of exhaust ducts. WC stands for "whole classroom."

Emitter level →	Low emitter		Medium emitter		High emitter		Superemitter	
	I	VI	I	VI	I	VI	I	VI
probability of infection ↓	Maximum radial distance (m)							
≥ 63%	Negligible risk of infection		⋯	⋯	0.80	0.80	6.53	7.16
≥ 50%			0.04	0.06	1.19	1.32	7.63	WC
≥ 25%			0.22	0.19	2.96	3.72	WC	WC
≥ 10%			0.77	0.81	6.15	6.86	WC	WC

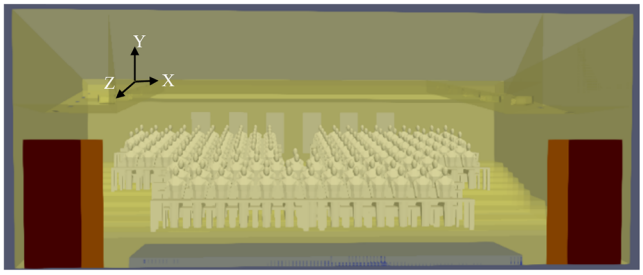

FIG. 14. Front view of the classroom with 168 occupants. The origin of the coordinate system is placed at the center of the domain.

TABLE IX. Parameters for simulating dispersion of pathogen in a room of capacity of 168 occupants.

Parameter	Value
Inlet air velocity (U)	1.8 m/s
Reynolds number (Re)	19 200
Volume of the room (V)	546.66 m^3
Area of flow inlet diffuser (A)	0.6×0.1275 m^2
Total air supply rate (Q)	1.377 m^3/s
Turbulent diffusion coefficient (Γ)	0.0299 m^2/s

exhaust ducts nearer to the floor on the side walls rather than on the ceiling, a strategy in contravention of the better air conditioning design. This is because the supply air from the ceiling sweeps away the pathogens downward, which are then easily removed by the exhaust ducts provided in the bottom of the side walls keeping in with the general flow of the air. Any other placement of the exhaust duct that does not obey this quasi-steady flow pattern of the air may increase the reach of the pathogen and prove detrimental to the health of the occupants.

Finally, the well-mixed approach assumes that the pathogen is spread evenly in the enclosed space and each person present has equal probability of getting infected. However, this work demonstrated that the spread of the pathogen inside the classroom is highly stratified. Based on the quanta of the pathogen as a function of distance from

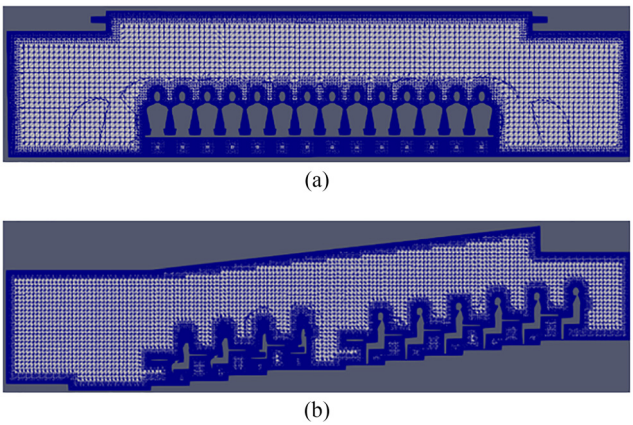

FIG. 15. Mesh of the 168 seater room shown in two different orthogonal planes. (a) Z = 0.4m. (b) X = 1.4 m.

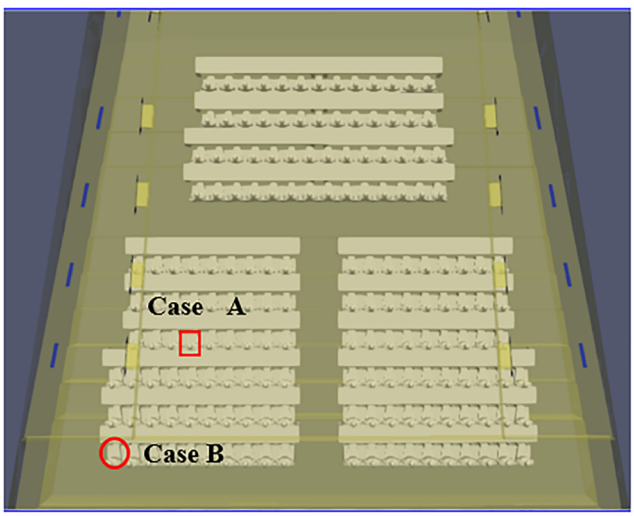

FIG. 16. Locations of the infected person considered for modeling of pathogen dispersion in the larger classroom.

TABLE XI. Comparison of number of susceptible students for different locations of the infected person.

	Susceptible persons	
Category	A	B
Low emitter	0	0
Medium emitter	1	1
High emitter	14	10
Superemitter	84	57

the emitter, it was estimated that it is crucial to maintain a distance of one meter between the occupants to reduce the chances of infection. This strategy, however, will not be beneficial in the case of a superemitter. In that case, everyone inside the room is highly susceptible to infection. Apart from keeping droplet transmission of the disease into mind, the aerosol transmission of the disease in enclosed spaces (particularly while dealing with the highly infectious diseases like SARS Cov-2) must also be considered while devising the policy framework for prevention of airborne diseases.

The results presented in this study were for dispersion of a general pathogen and not just limited to SARS-Cov-2. Hence, our findings will also be applicable for situations where the effective diffusivity Γ is similar. Furthermore, our results obtained by modeling dispersion in two different size rooms provide a common finding that the "one-meter-distance" rule is a good guideline for reducing the probability of getting infected and this will be applicable to other indoor scenarios as well. However, it is worthwhile to mention that this work has been a first effort in modeling the aerosol dispersion of the pathogen exhaled by breathing in a large, indoor space with large number of occupants. The simulations were highly complex owing to the large computational domain size and wide variety of complex geometric features, which needed to be resolved while modeling humans and inlet diffusers in the space considered in this work. For computational convenience, the variation of temperature in the domain has been neglected. However, any future work may include the effect of temperature change inside the domain. Furthermore, an experimental study to correlate the findings of the study could be carried out by placing a source, which imitates the aerosol emission by human breathing and placing human mannequins, furniture, and probes.

TABLE X. Comparison of the probability of infection with distance for different locations of infected person for an exposure of one hour.

Emitter level →	Low emitter		Medium emitter		High emitter		Superemitter	
	A	B	A	B	A	B	A	B
probability of infection ↓	Maximum radial distance (m)							
≥63%	Negligible risk of infection		···	···	···	0.50	7.73	5.12
≥50%			···	···	0.04	1.22	10.43	5.58
≥25%			···	0.06	1.71	3.46	10.43	12.63
≥10%			···	0.44	7.03	5.01	12.5	13.48

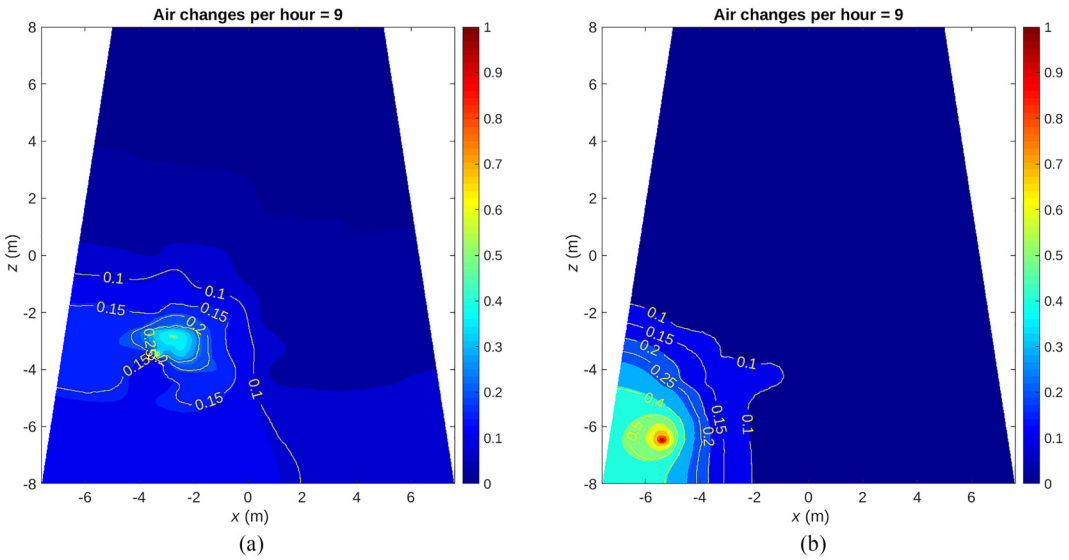

FIG. 17. Probability of spread of infection with different locations of infected person in the case of a high emitter. (a) Case A. (b) Case B.

AUTHOR DECLARATIONS

Conflict of Interest

The authors have no conflicts to disclose.

Author Contributions

Praveen Sharma: Data curation (lead); Formal analysis (lead); Investigation (lead); Methodology (equal); Software (lead); Validation (lead); Visualization (lead); Writing – original draft (lead); Writing – review & editing (equal). **Supreet Singh Bahga:** Conceptualization (supporting); Methodology (supporting); Supervision (supporting); Writing – review & editing (supporting). **Amit Gupta:** Conceptualization (equal); Methodology (equal); Supervision (equal); Writing – review & editing (equal).

DATA AVAILABILITY

The data that support the findings of this study are available from the corresponding author upon reasonable request.

APPENDIX: TURBULENCE MODEL

1. The $k-\epsilon$ model

The fluctuation effect of the turbulent effect is taken into account by the RANS equations. These equations govern the mean velocity field. The velocity in a turbulent field can be decomposed into its mean and fluctuating component using Reynolds decomposition[44]

$$\vec{\mathrm{U}}(\mathrm{x},\mathrm{t}) = \left\langle \vec{U}(x,t) \right\rangle + \vec{\mathrm{u}}(\mathrm{x},\mathrm{t}), \tag{A1}$$

where $\vec{U}(x,t) = \text{velocity field}$, $\left\langle \vec{U}(x,t) \right\rangle = \text{ensemble} - \text{averaged velocity field}$, and $\vec{u}(x,t) = \text{fluctuation part}$.

Averaging the Navier–Stokes equation, we obtain the mean momentum or Reynolds averaged Navier–Stokes (RANS) equations,

$$\frac{\overline{D}\langle U_j \rangle}{\overline{D}t} = \nu \nabla^2 \langle U_j \rangle - \frac{\partial \langle u_i u_j \rangle}{\partial x_i} - \frac{1}{\rho}\frac{\partial \langle p \rangle}{\partial x_j}, \tag{A2}$$

where $\nu =$ kinematic viscosity and $\rho =$ density and $\frac{\overline{D}}{\overline{D}t}$ is the material or mean substantial derivative and is equivalent to

$$\frac{\overline{D}}{\overline{D}t} = \frac{\partial}{\partial t} + \langle \vec{U} \rangle \cdot \nabla$$

The terms on the right side consist of the viscous stresses, the isotropic stresses from the mean pressure field and the apparent stress known as Reynolds stress, $(\rho \langle u_i u_j \rangle)$, arising from the fluctuating velocity field. These equations pose the closure problem, and hence, the k-ϵ model is used for closure of these equations.

The $k-\epsilon$ model is a two-equation model. The transport equations are solved for two turbulence quantities, i.e., k and ϵ. It is the most widely used turbulence model and is incorporated in most commercial CFD solvers. The model consists of the following equations.

(a) The model transport equation for the turbulent kinetic energy, k, is

$$\frac{\overline{D}k}{\overline{D}t} = \nabla \cdot \left(\frac{\nu_T}{\sigma_k} \nabla k \right) + \mathrm{p} - \epsilon, \tag{A3}$$

where ϵ is the dissipation, p is the turbulent kinetic energy production, and σ_k is the turbulent Prandtl number.

(b) The model transport equation for dissipation, ϵ, is

$$\frac{\overline{D}\epsilon}{\overline{D}t} = \nabla \cdot \left(\frac{\nu_T}{\sigma_\epsilon} \nabla \epsilon \right) + \frac{C_{\epsilon 1}\mathrm{p}\epsilon}{\mathrm{k}} - \frac{C_{\epsilon 2}\epsilon^2}{\mathrm{k}}. \tag{A4}$$

(c) The turbulent viscosity is given as

$$\nu_T = \frac{C_\mu k^2}{\epsilon}. \tag{A5}$$

The standard values of the model constants are as follows:[44]

$$C_\mu = 0.09, C_{\epsilon 1} = 1.44, C_{\epsilon 2} = 1.92, \sigma_k = 1.0, \text{ and } \sigma_\epsilon = 1.3.$$

REFERENCES

[1]H. Lu, C. W. Stratton, and Y. W. Tang, "Outbreak of Pneumonia of unknown etiology in Wuhan, China: The mystery and the miracle," J. Med. Virol. **92**(4), 401–402 (2020).

[2]See https://www.worldometers.infor/coronavirus/ for "WorldoMeter."

[3]J. A. Lednicky, M. Lauzard, Z. H. Fan, A. Jutla, T. B. Tilly, M. Gangwar, M. Usmani, S. N. Shankar, K. Mohamed, A. Eiguren-Fernandez, C. J. Stephenson, Md. Mahbubul Alam, M. A. Elbadry, J. C. Loeb, K. Subramaniam, T. B. Waltzek, K. Cherabuddi, J. Glenn Morris Jr., and C. Y. Wu, "Viable SARS-CoV-2 in the air of a hospital room with COVID-19 patients," Int. J. Infect. Dis. **100**, 476–482 (2020).

[4]L. Morawska and J. Cao, "Airborne transmission of SARS COV-2: The world should face the reality," Environ. Int. **139**, 105730 (2020).

[5]M. Jayaweera, H. Perera, B. Gunawardana, and J. Manatunge, "Transmission of COVID-19 virus by droplets and aerosols: A critical review on the unresolved dichotomy," Environ. Res. **188**, 109819 (2020).

[6]M. Z. Bazant and J. W. M. Bush, "A guideline to limit indoor airborne transmission of COVID-19," Proc. Natl. Acad. Sci. U. S. A. **118**(17), e2018995118 (2021).

[7]World Health Organisation, see https://apps.who.int/iris/bitstream/handle/10665/112656/9789241507134_eng.pdf?sequence=1 for "Infection Prevention and Control of Epidemic- and Pandemic-Prone Acute Respiratory Infections in Health Care (2014).

[8]W. F. Wells, "ON AIR-borne infection: Study II. Droplets and droplet nuclei," Am. J. Epidemiol. **20**(3), 611–618 (1934).

[9]J. P. Duguid, "The size and the duration of air-carriage of respiratory droplets and droplet-nuclei," Epidemiol. Infect. **44**(6), 471–479 (1946).

[10]R. Dhand and J. Li, "Coughs and sneezes: Their role in transmission of respiratory viral infections, Including SARS CoV-2," Am. J. Respir. Crit. Care Med. **202**(5), 651–659 (2020).

[11]R. S. Papineni and F. S. Rosenthal, "The size distribution of droplets in the exhaled breath of healthy human subjects," J. Aerosol Med. **10**(2), 105–116 (1997).

[12]L. Morawska, G. R. Johnson, Z. D. Ristovski, M. Hargreaves, K. Mengersen, S. Corbett, C. Y. H. Chao, Y. Li, and D. Katoshevski, "Size distribution and sites of origin of droplets expelled from the human respiratory tract during expiratory activities," J. Aerosol Sci. **40**(3), 256–269 (2009).

[13]X. Xie, Y. Li, A. T. Y. Chwang, P. L. Ho, and W. H. Seto, "How far droplets can move in indoor environments–revisiting the Wells evaporation-falling curve," Indoor Air **17**(3), 211–225 (2007).

[14]R. Mittal, R. Ni, and J. H. Seo, "The flow physics of COVID-19," J. Fluid Mech. **894**, F2 (2020).

[15]S. A. Chillón, A. Ugarte-Anero, I. Aramendia Iradi, U. Fernandez-Gamiz, and E. Zulueta, "Numerical modelling of the spread of cough saliva droplets in a calm confined space," Mathematics **9**(5), 574 (2021).

[16]T. Dbouk and D. Drikakis, "On coughing and airborne droplet transmission to humans," Phys. Fluids **32**(5), 053310 (2020).

[17]M. Rezaali and R. Fouladi-Fard, "Aerosolized SARS-CoV-2 exposure assessment: Dispersion modelling with AERMOD," J. Environ. Health Sci. Eng. **19**(1), 285–293 (2021).

[18]L. Bourouiba, E. Dehandschoewercker, and J. W. M. Bush, "Violent expiratory events: On coughing and sneezing," J. Fluid Mech. **745**, 537–563 (2014).

[19]L. Bourouiba, "Turbulent gas clouds and respiratory pathogen emissions: Potential implications for reducing transmission of COVID-91," JAMA **323**(18), 1837–1838 (2020).

[20]L. Bourouiba, "The fluid dynamics of disease transmission," Annu. Rev. Fluid Mech. **53**, 473–508 (2021).

[21]L. Borro, L. Mazzei, M. Raponi, P. Piscitelli, A. Miani, and A. Secinaro, "The role of air conditioning in the diffusion of Sars-CoV-2 in indoor environments: A first computational fluid dynamic model, based on investigations performed at the Vatican State Children's hospital," Environ. Res. **193**, 110343 (2021).

[22]Y. Zhang, G. Feng, Z. Kang, Y. Bi, and Y. Cai, "Numerical simulation of coughed droplets in conference room," Procedia Eng. **205**, 302–308 (2017).

[23]M. R. Pendar and J. Carlos Páscoa, "Numerical modelling of the distribution of virus carrying saliva droplets during sneeze and cough," Phys. Fluids **32**(8), 083305 (2020).

[24]A. A. Aliabadi, S. N. Rogak, S. I. Green, and K. H. Bartlett, "CFD simulation of human coughs and sneezes: A study in droplet dispersion, heat, and mass transfer," in *ASME International Mechanical Engineering Congress and Exposition* (ASME, 2010), pp. 1051–1060.

[25]H. Li, F. W. Leong, G. Xu, Z. Ge, C. W. Kang, and K. H. Lim, "Dispersion of evaporating cough droplets in tropical outdoor environment," Phys. Fluids **32**(11), 113301 (2020).

[26]N. Van Doremalen, T. Bushmaker, D. H. Morris, M. G. Holbrook, A. Gamble, B. N. Williamson, A. Tamin, J. L. Harcourt, N. J. Thornburg, S. I. Gerber, J. O. Lloyd-Smith, E. de Wit, and V. J. Munster, "Aerosol and surface stability of SARS-CoV-2 as compared with SARS-CoV-1," N. Engl. J. Med. **382**(16), 1564–1567 (2020).

[27]N. R. de Sousa, L. Steponaviciute, L. Margerie, K. Nissen, M. Kjellin, B. Reinius, E. Salaneck, K. I. Udekwu, and A. G. Rothfuchs, "Detection and isolation of airborne SARS-CoV-2 in a hospital setting," Indoor Air **32**(3), e13023 (2022).

[28]C. F. Picard, L. C. R. Salis, and M. Abadie, "Home quarantine: A numerical evaluation of SARS-CoV-2 spread in a single-family house," Indoor Air **32**(5), e13035 (2022).

[29]K. Sinha, M. S. Yadav, U. Verma, J. S. Muralidharan, and V. Kumar, "Effect of recirculation zones on the ventilation of a public washroom," Phys. Fluids **33**(11), 117101 (2021).

[30]A. Venkatram and J. Weil, "Modelling turbulent transport of aerosols inside rooms using eddy diffusivity," Indoor Air **31**(6), 1886–1895 (2021).

[31]S. L. Miller, W. W. Nazaroff, J. L. Jimenez, A. Boerstra, G. Buonanno, S. J. Dancer, J. Kurnitski, L. C. Marr, L. Morawska, and C. Noakes, "Transmission of SARS-CoV-2 by inhalation of respiratory aerosol in the Skagit Valley Chorale superspreading event," Indoor Air **31**(2), 314–323 (2021).

[32]J. Yan, M. Grantham, J. Pantelic, P. De Mesquita, B. Albert, F. Liu, and E. S. D. Milton, and E. Consortium, "Infectious virus in exhaled breath of symptomatic seasonal influenza cases from a college community," Proc. Natl. Acad. Sci. U. S. A. **115**(5), 1081–1086 (2018).

[33]G. R. Johnson and L. Morawska, "The mechanism of the breath aerosol formation," J. Aerosol Med. Pulm. Drug Delivery **22**(3), 229–237 (2009).

[34]J. Fiegel, R. Clarke, and D. Edwards, "Airborne infectious disease and the suppression of pulmonary bioaerosols," Drug Discovery Today **11**(1–2), 51–57 (2006).

[35]M. Atkinson and L. Wein, "Quantifying the routes of transmission for pandemic influenza," Bull. Math. Biol. **70**(3), 820–867 (2008).

[36]R. Zhang, Y. Li, A. Zhang, Y. Wang, and M. Molina, "Identifying airborne transmission as the dominant route for the spread of COVID-19," Proc. Natl. Acad. Sci. U. S. A. **117**(2), 14857–14863 (2020).

[37]S. Asadi, A. Wexler, C. Cappa, S. Barreda, N. Bouvier, and W. Ristenpart, "Aerosol emission and superemission during human speech increase with voice loudness," Sci. Rep. **9**(1), 2348 (2019).

[38]J. Gralton, E. Tovey, M. McLaws, and W. Rawlinson, "The role of particle size in aerosolised pathogen transmission: A review," J. Infection **62**(1), 1–13 (2011).

[39]R. Mittal, C. Meneveau, and W. Wu, "A mathematical framework for estimating risk of airborne transmission of COVID-19 with application to face mask use and social distancing," Phys. Fluids **32**(10), 101903 (2020).

[40]G. Buonanno, L. Stabile, and L. Morawska, "Estimation of airborne viral emission: Quanta emission rate of SARS-CoV-2 for infection risk assessment," Environ. Int. **141**, 105794 (2020).

[41]H. Hanzawa, A. K. Melikov, and P. O. Fanger, "Airflow characteristics in the occupied zone of ventilated spaces," in *ASHRAE Transactions: Technical and Symposium Papers Presented at the 1987 Winter Meeting* (ASHRAE, 1987), Vol. 93, No. 1, pp. 524–539.

[42]Y. Xia, J. Niu, R. Zhao, and J. Burnett, "Effects of turbulent air on human thermal sensations in a warm isothermal environment," Indoor Air **10**(4), 289–296 (2000).
[43]G. Johnson, L. Morawska, Z. Ristovski, M. Hargreaves, K. Mengersen, C. Chao, M. Wan, Y. Li, X. Xie, D. Katoshevski, and S. Corbett, "Modality of human expired aerosol size distributions," J. Aerosol Sci. **42**(12), 839–851 (2011).
[44]S. Pope, *Turbulent Flows* (Cambridge University Press, New Delhi, 2000).
[45]T. Hussein, J. Löndahl, S. Thuresson, M. Alsved, A. Al-Hunaiti, K. Saksela, H. Aqel, H. Junninen, A. Mahura, and M. Kulmala, "Indoor model simulation for COVID-19 transport and exposure," Int. J. Environ. Res. Public Health **18**(6), 2927 (2021).
[46]S. Karimzadeh, R. Bhopal, and H. Tien, "Review of infective dose, routes of transmission and outcome of COVID-19 caused by the SARS-COV-2: Comparison with other respiratory viruses," Epidemiol. Infect. **149**, e96 (2021).
[47]M. Riediker and D. Tsai, "Estimation of viral aerosol emissions from simulated individuals with asymptomatic to moderate coronavirus disease 2019," JAMA Network Open **3**(7), e2013807 (2020).
[48]J. Ma, X. Qi, and H. Chen, "COVID-19 patients in earlier stages exhaled millions of SARS-CoV-2 per hour," Clin. Infect. Dis. **72**(10), e652–e654 (2020).
[49]M. Malik, A. C. Kunze, T. Bahmer, S. Herget-Rosenthal, and T. Kunze, "SARS-CoV-2: Viral loads of exhaled breath and oronasopharyngeal specimens in hospitalized patients with COVID-19," Int. J. Infect. Dis. **110**, 105–110 (2021).
[50]R. Wölfel, V. Corman, W. Guggemos, M. Seilmaier, S. Zange, M. Müller, D. Niemeyer, T. Jones, P. Vollmar, C. Rothe, and M. Hoelscher, "Virological assessment of hospitalized patients with COVID-2019," Nature **581**(7809), 465–469 (2020).
[51]Y. Pan, D. Zhang, P. Yang, L. Poon, and Q. Wang, "Viral load of SARS-CoV-2 in clinical samples," Lancet Infect. Dis. **20**(4), 411–412 (2020).
[52]K. K. W. To, O. T. Y. Tsang, W. S. Leung, A. R. Tam, T. C. Wu, D. C. Lung, C. C. Y. Yip, J. P. Cai, J. M. C. Chan, T. S. H. Chik, and D. P. L. Lau, "Temporal profiles of viral load in posterior oropharyngeal saliva samples and serum antibody responses during infection by SARS-CoV-2: An observational cohort study," Lancet Infect. Dis. **20**(5), 565–574 (2020).
[53]T. Foat, J. Drodge, J. Nally, and S. Parker, "A relationship for the diffusion coefficient in eddy diffusion based indoor dispersion modelling," Build. Environ. **169**, 10659 (2020).
[54]A. Prasad and J. Koseff, "Reynolds number and end-wall effects on a lid-driven cavity flow," Phys. Fluids A **1**(2), 208–218 (1989).
[55]P. Shankar and M. Deshpande, "Fluid mechanics in the driven cavity," Annu. Rev. Fluid Mech. **32**(1), 93–136 (2000).
[56]J. Wang and D. Wan, "Parallel simulation of 3D lid driven cubical cavity flows using finite element analysis," in Proceedings of the Twenty First International Offshore and Polar Engineering Conference, 2011.
[57]E. Leriche and S. Gavrilakis, "Direct numerical simulation of the flow in a lid-driven cubical cavity," Phys. Fluids **12**(6), 1363–1376 (1989).
[58]E. Leriche, "Direct numerical simulation in a lid driven cubical cavity at high Reynolds number by a Chebyshev spectral method," J. Sci. Comput. **27**(1–3), 335–345 (2006).
[59]R. Zhang, C. Zhong, S. Liu, and C. Zhuo, "Large-eddy simulation of wall bounded turbulent flow with high order discreet unified gas kinetic scheme," Adv. Aerodyn. **2**, 1–27 (2020).
[60]R. Bouffanais, M. Deville, and E. Leriche, "Large-eddy simulation of the flow in a lid driven cubical cavity," Phys. Fluids **19**, 055108 (2007).
[61]See https://courses.lumenlearning.com/wm-biology2/chapter/breathing-capacity/ for information about air inhaled during a normal breath.
[62]L. Warliah, A. Rohman, and P. Rusmin, "Model development of air volume and breathing frequency in human respiratory system simulation," Procedia Social Behav. Sci. **67**, 260–268 (2011).
[63]J. Gupta, C. Lin, and Q. Chen, "Characterizing exhaled airflow from breathing and talking," Indoor Air **20**(1), 31–39 (2010).
[64]V. Arumuru, J. Pasa, S. Samantaray, and V. Varma, "Breathing, virus transmission, and social distancing—An experimental visualization study," AIP Adv. **11**(4), 045205 (2021).
[65]C. Noakes, C. Beggs, P. Sleigh, and K. Kerr, "Modelling the transmission of airborne infections in enclosed spaces," Epidemiol. Infect. **134**(5), 1082–1091 (2006).
[66]See www.ashrae.org for "Guidance for the Re-opening of Schools, ASHRAE (2020)" (last accessed August 20, 2020).